

# Driving Force and Thermal Activation in Martensite Kinetics

J.R.C. GUIMARÃES and P.R. RIOS

A formal kinetics equation derived by the authors in previous work to provide a unified description of martensite transformation is applied to martensite transformation curves obtained with different iron-base alloys under different conditions. In previous work, our formalism was shown to describe athermal as well as isothermal martensite transformation. In this work, it is demonstrated that our unified formalism is able to describe isothermal martensite transformation under depressurization, in the presence of a magnetic field and induced by applied strain. We found that the values of the apparent activation energy fall roughly within an order of magnitude and are compatible with the results reported in the literature. Other important features of martensite transformations, such as, martensite embryos, autocatalysis, and chemical driving force are also discussed. We suggest that our findings are qualitatively compatible with the view that in a favorable environment, austenite can evolve into metastable embryos that are promoted to nuclei, eventually. The embryo→nuclei transition could be regulated by a small barrier overcome by thermal activation.

DOI: 10.1007/s11661-009-9902-5

© The Minerals, Metals & Materials Society and ASM International 2009

## I. INTRODUCTION

THE properties of engineering steels during production, manufacturing, and use depend upon our ability to exert microstructure control. Among other means, martensite transformation has been proven especially useful. However, martensite is not as trivial as the previous sentence may convey. Although vintage abaci and compilations have been replaced by modern data bases, so did the complexity of issues emerging from the development of new steels and steel usage, a scenario that supports further delving fundamental aspects of martensite particularly in steels.

Martensite in steels is typically heterogeneous and autocatalytic. The reaction proceeds by the nucleation of new units instead of growth of a few ones. Observation of plates in self-accommodating “zig-zag” patterns is common, as shown in Figure 1. The reaction kinetics responds to mechanical stimuli, hydrostatic pressure, and magnetic fields, as will be discussed in Sections IV through VI.

The usefulness of classical homogeneous nucleation concepts to martensite was questioned early as the approach failed in providing a unified view of the perceived characteristics of martensite kinetics. To cope with the issues, it has been postulated that compositional<sup>[1]</sup> or structural martensite embryos<sup>[2]</sup> be part of the nucleation process. The second type of embryo has been further developed. In the meantime, acknowledged

crystallographic aspects of martensite pointed out that the martensite-austenite interface should be semicoherent.<sup>[3]</sup> Extension of the concept to the realm of the martensite nucleus yielded a nucleation barrier that would not be overcome by thermal fluctuations alone.<sup>[4]</sup> This led to relocation of the critical barrier from austenite→martensite to embryo→martensite. Single-domain embryos with semicoherent interfaces were assumed to propagate into martensite by punching out dislocation loops to maintain semicoherence. The calculated activation energy for this process is much less than the overall nucleation barrier for a semicoherent nucleus. A linear relationship between the activation energy for nucleation and driving force is a characteristic of the model.<sup>[4]</sup>

Later, Olson<sup>[5]</sup> proposed a reaction path comprising the dissociation of an austenite defect into a bcc fault assembly driven by the available free energy. Propagation into martensite would become barrierless for a negative fault energy. The process requires dislocation motion (the partials bounding the fault); hence, it depends on thermal activation that may lead to time-dependent transformation. A linear relationship between activation energy and driving force is also predicted.

Meyers<sup>[6]</sup> considered dynamic aspects of the growth of martensite. A nucleus should be formed in a highly compressed state. Propagation of such nucleus generates two coupled waves (longitudinal and transverse with respect to the plate's midplane). The longitudinal wave generates the midrib and activates a transverse wave that transforms austenite into martensite (thickening) until it is overcome by attenuation. Transformation strains imposed in the surrounding austenite in a wavelike manner by the transverse wave and the resultant debris are partially inherited by the martensite plates, as corroborated by Shibata *et al.*<sup>[7]</sup>

Ghosh and Olson<sup>[8]</sup> analyzed the mobility of the martensite-austenite interface as the critical step in the

---

J.R.C. GUIMARÃES, (ret) Researcher at Large, is with the Escola de Engenharia Industrial Metalúrgica de Volta Redonda, Universidade Federal Fluminense, 27255-125, Volta Redonda, RJ, Brazil, and Mal. Moura 338H/22C, 05641-000, São Paulo, SP, Brazil. P.R. RIOS, Professor, is with the Escola de Engenharia Industrial Metalúrgica de Volta Redonda, Universidade Federal Fluminense. Contact e-mail: prrios@metal.eeimvr.uff.br

Manuscript submitted February 14, 2009.

Article published online August 19, 2009

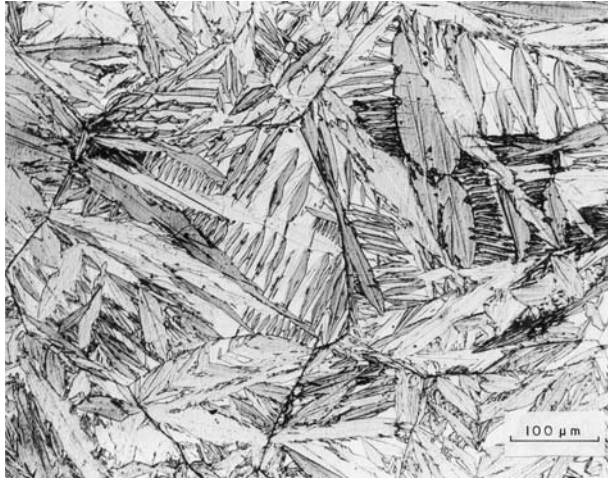


Fig. 1—Martensite plates in Fe-31.9 mass pct Ni-0.02 mass pct C athermally transformed during cooling to 77 K.

heterogeneous barrierless nucleation of martensite pursuing a propagation concept described by Magee.<sup>[9]</sup> Their computations indicate that the composition dependence of the athermal frictional work for the martensite interface is of the same form as that for slip deformation. It is noteworthy that the model described the compositional dependence of the martensite start temperature in multicomponent alloys with an accuracy of  $\pm 40$  K.

Kakeshita *et al.*<sup>[10–12]</sup> brought up a unified rationalization of the time-dependent and time-independent modes of martensite transformation, in which relevant particles (atom, electron) must acquire a certain critical energy to change the state from austenite to martensite. The transition probability is given by a Boltzmann factor with a free energy of activation determined by the difference between the driving force to start martensite and the difference in Gibbs free energy between martensite and austenite. However, transformation is only observed when a cluster of excited particles exists in the austenite. The volume of a cluster was estimated to be at most  $2 \text{ nm}^3$ . It is noteworthy that nucleation of multi-domain units in iron alloys and steels<sup>[13]</sup> has been found to be compatible with a nucleation barrier  $\frac{1}{1000}$  of the magnitude of the nucleation barrier estimated for homogenous nucleation of single domain nuclei.<sup>[4]</sup> More recently, a phase field microelasticity model of heterogeneous martensite transformation<sup>[14,15]</sup> incorporated in its construction this idea that in a favorable environment austenite may evolve into embryos. According to this model, those embryos, made of stress accommodating microdomains, could be either metastable or unstable and propagate barrierless. The former embryos demand thermal activation to propagate.

This brief summary highlights significant advances in the understanding of fundamental aspects of martensite kinetics. It is clear that, in spite of progress achieved in the understanding of martensite, formal issues relating to the different kinetic modes of martensite transformation are still relevant.<sup>[16–20]</sup>

In previous work,<sup>[19,20]</sup> the present authors developed a formal approach to discuss the kinetics of the

initiation<sup>[19]</sup> and subsequent evolution<sup>[20]</sup> of martensite transformation. The theory provides a unified description of martensite microstructure and transformation curve and was successfully applied to both athermal and isothermal martensite.

In the present work, we show that such a unified description also applies to isothermal martensite transformations in which austenite is subjected to depressurization, magnetic field, or applied strain. Martensite transformation by and large has been studied with focus on certain alloys and experimental conditions. Specifically, we analyze data from transformation curves of isothermal martensite induced in martensite iron-base alloys by different means.

## II. INITIATION OF MARTENSITIC TRANSFORMATION

The small particle experiment of Cech and Turnbull<sup>[21]</sup> demonstrated that austenite particles from the same alloy start transforming at different temperatures, stressing that nucleation sites are initially scarce and not equipotent.

The probability that at least one nucleation site exists in a particle of mean volume  $q$  is exponentially related to the number per unit volume of material of sites for martensite nucleation available to propagate down to temperature  $T$ :<sup>[22]</sup>

$$P_q(T) = 1 - \exp(-q \cdot n_V^T) \quad [1]$$

The value of  $P_q(T)$  may be equated to the volume fraction of material in partially transformed particles. The values of  $n_V^T$ , obtained by fitting the data from Cech and Turnbull<sup>[21]</sup> with Eq. [1], were shown to correlate with the reaction driving force,  $\Delta G$ , and the temperature  $T$ <sup>[19]</sup> using the following expression:

$$n_V^T = n_V^0 \left( \frac{\Delta G - \Delta G_0}{kT} \right) \quad [2]$$

where  $n_V^0$  stands for the value of  $n_V^T$  when  $\Delta G - \Delta G_0 = kT$ . The product  $kT$  was used in Eq. [2] to homogenize units. The term  $\Delta G_0$  is a critical value of the chemical driving force for nucleation sites becoming viable martensite embryos. In order to avoid possible confusion, it is important to clarify that we denote the driving force, which is defined as usual as minus the free energy change of austenite to martensite transformation. Therefore, the driving force is a positive quantity in spontaneous transformations.

Equation [2] does not distinguish whether martensite kinetics is time dependent. It is worth noting that the value of  $n_V^0$  can be influenced by thermomechanical treatment, by autocatalysis, or by an external field. The values of  $n_V^T$  determined by fitting the small particle transformation data with Eq. [2] do not reflect the counted nucleation sites but actual nucleation events; that is, they relate to the conversion of embryos into nuclei. Henceforth, the ratio  $\frac{\Delta G - \Delta G_0}{kT}$  gives the factor by which driving force and temperature influence the

density of nuclei. If the conversion of embryos into nuclei were thermally activated, the density of nuclei would be proportional to  $\frac{\Delta G - \Delta G_0}{kT} \exp\left(-\frac{E_p}{kT}\right)$ . The expression is model dependent, although, formally, it fits the framework of absolute rate theory applied to isothermal martensite<sup>[23]</sup> as well as being in agreement with the concepts described in References 10 through 12. Let  $\xi$  be the experimental variable, *e.g.*, time or strain. The  $\xi$ -rate of change of the number per unit volume of martensite units isothermally formed at temperature  $T$  is formally written as

$$\frac{dN_V}{d\xi} = n_V^T (1 - V_V) R_\xi \quad [3]$$

where  $V_V$  is the martensite volume fraction and  $R_\xi$  the rate factor. If thermal activation is involved,

$$R_\xi = \frac{\nu}{\dot{\xi}} \exp\left(-\frac{E_p}{kT}\right) \quad [4]$$

where  $\nu$  is the lattice frequency,  $\dot{\xi}$  is the time-rate of change of  $\xi$ , and  $E_p$  is an apparent activation energy.

Combining Eqs. [2] through [4] gives

$$\frac{dN_V}{d\xi} = n_V^0 \left(\frac{\Delta G - \Delta G_0}{kT}\right) (1 - V_V) \frac{\nu}{\dot{\xi}} \exp\left(-\frac{E_p}{kT}\right) \quad [5]$$

Since the ratio  $\frac{\Delta G - \Delta G_0}{kT}$  increases with increasing driving force beyond  $\Delta G_0$  or decreasing temperature, a ‘‘C-curve behavior’’ can be described by Eq. [5]. This has been demonstrated<sup>[19]</sup> by considering the initial rate (at 0.002 fraction transformed) of isothermal martensite ( $\xi = \text{time}$ ) in Fe-23.2 mass pct Ni-2.8 mass pct Mn.<sup>[24]</sup> The values of the parameters in Eq. [5], obtained in Reference 19, are repeated here for convenience:  $n_V^0 = 3800 \text{ m}^{-3}$ ,  $\Delta G_0 = 2.9 \cdot 10^{-21} \text{ J-event}^{-1}$ , and  $E_p = 7.5 \cdot 10^{-21} \text{ J-event}^{-1}$ .

It is noteworthy that the value of  $E_p$  is similar in magnitude to the activation energy  $\approx 4 \cdot 10^{-21} \text{ J-event}^{-1}$  for the ‘‘growth of a martensite embryo’’ obtained by Kurdjumov and Maximova.<sup>[25,26]</sup> As already mentioned, the value of  $n_V^0$  can be influenced by thermomechanical treatment, by autocatalysis, or by an external field. As a matter of fact, the value of  $n_V^0$  obtained in Eq. [19] is significantly distinct from the  $10^{13} \text{ m}^{-3}$  generally admitted for the density of initial available nucleation sites.

In a previous article,<sup>[20]</sup> the present authors have shown that an expression for  $n_V^0$  compatible with the reaction condition, Eqs. [2] and [5], could be applied to describe the transformation curves of FeNiMn isothermally transformed as well as that of FeNiC athermally transformed by quenching below  $M_s$ .

### III. EVOLUTION OF MARTENSITIC TRANSFORMATION

The model development required an analytical description of the volume fraction transformed,  $V_V$ , as a function of the number per unit volume,  $N_V$ , of

martensite units. The underlying assumption of the analytical model advanced in Eq. [20] to convert number per unit volume into volume fraction transformed,  $V_V = \Phi(N_V)$ , is that, factually, the diameter of a martensite midplane is limited by the size of the untransformed austenite volume where it forms. Thus, the length of a newly formed midrib can be considered an estimator of the mean free distance observed on a polished section of a partially transformed material. As a result, the number per unit volume of martensite plates,  $N_V$ , and the area of martensite midplanes,  $S_{V,m}$ , are related as<sup>[20]</sup>

$$N_V = \frac{\pi}{48} \left( (S_{V,m} + S_{V,\gamma})^3 - S_{V,\gamma}^3 \right) \quad [6]$$

where  $S_{V,\gamma}$  is the area per unit volume of internal boundaries in the austenite. Equation [6] has no adjustable parameters. For martensite plates with the shape of slender oblate spheroids of aspect ratio  $\alpha$ ,<sup>[20]</sup>

$$V_V = \frac{16\alpha}{9\pi} \ln \left( 1 + \frac{48N_V}{\pi S_{V,\gamma}^3} \right) \quad [7]$$

The validation of this equation was accomplished as described in Reference 20. However, Eq. [7] probably does not work when the austenite grain size becomes very small. In this case, the reaction pattern resembles that observed with a particulate.<sup>[21]</sup> Martensite units are initially contained in a few clustered grains. Subsequently new clusters are formed elsewhere, spreading the reaction throughout the material. This aspect of martensite transformation has been named ‘‘spread.’’<sup>[27]</sup> It has been shown that during spreading, it is realistic to admit that the mean plate volume,  $\bar{v}$ , remains constant<sup>[28]</sup> and  $V_V = \bar{v}N_V$  can be used instead of Eq. [7].

Autocatalysis is foremost regarding the shape of a martensite transformation curve. Actually, autocatalysis is effective from the beginning of the reaction. During spreading, autocatalysis can be operationally described by a unitless parameter, as discussed elsewhere.<sup>[29]</sup> However, a more complex situation exists when the martensite units form mainly between existing plates, *e.g.*, in partially-transformed coarse-grained austenite. Autocatalysis under such ‘‘fill-in’’ condition has been described as a volume effect,<sup>[30,31]</sup> although, admittedly,<sup>[32,33]</sup> the martensite-austenite interface should be expected to have a role in that. The propagation of a martensite plate introduces debris in the surrounding austenite, which interact with the thickening plate.<sup>[6,7,34]</sup> Thus, the martensite-austenite interface must have an effect on the availability of autocatalytic nucleation sites. Assuming that autocatalysis is dominant,<sup>[20]</sup> the product  $a_{ac}S_{V,m\gamma}$  replaces  $n_V^0$  in Eq. [2], giving us

$$n_V^T = a_{ac} S_{V,m\gamma} \left( \frac{\Delta G - \Delta G_0}{kT} \right) \quad [8]$$

where  $a_{ac}$  is an autocatalytic scale factor per unit area of martensite-austenite interfaces, and  $S_{V,m\gamma}$  is the area per unit volume of martensite-austenite interfaces. For slender oblate spheroids,  $S_{V,m\gamma} = 2S_{V,m}(1 - V_V)$ ,



where the term  $1 - V_V$  accounts for plate-on-plate impingement. Therefore, Eq. [8] becomes  $S_{V,m}$ :

$$n_{V,ac}^T = 2a_{ac}S_{V,m}(1 - V_V)\left(\frac{\Delta G - \Delta G_0}{kT}\right) \quad [9]$$

Combining Eqs. [5], [7], and [9] and recalling that  $\Delta G$  is nearly linear dependent on temperature in the range relevant to martensite transformation in steels gives us the following expression for the transformation curve:

$$\int \frac{9\pi \exp\left(\frac{9\pi V_V}{16\alpha}\right)}{16\alpha(\exp\left(\frac{3\pi V_V}{16\alpha}\right) - 1)} dV_V = A \int \frac{\Delta S}{k} \left(\frac{T^* - T}{T}\right)^{\frac{v}{\xi}} \exp\left(-\frac{E_p}{kT}\right) d\xi \quad [10]$$

where  $A = \frac{96a_{ac}}{\pi S_{V,\gamma}^2}$ ,  $\Delta S$  is the entropy change,  $k$  is the Boltzmann constant, and  $T^*$  is the temperature at which  $\Delta G(T^*) = \Delta G_0$ .

During ‘‘spread,’’ it should be apparent that the importance of the initially available sites is not entirely overwhelmed by autocatalysis. To account for that, autocatalysis has been operationally described by a unitless factor,<sup>[29]</sup>  $a_{ac}^s$ . Henceforth, Eq. [2] becomes

$$n_{V,ac}^T = a_{ac}^s(1 - V_V)n_V^0\left(\frac{\Delta G - \Delta G_0}{kT}\right) \quad [11]$$

Making the approximation  $V_V = \bar{v}N_V$ , the analog of Eq. [10] during spreading is

$$\int \frac{dV_V}{(1 - V_V)} = A^S \int \frac{\Delta S}{k} \left(\frac{T^* - T}{T}\right)^{\frac{v}{\xi}} \exp\left(-\frac{E_p}{kT}\right) d\xi \quad [12]$$

where  $A^S = n_V^0 a_{ac}^s \bar{v}$ .

In the following sections, we rely on data that have been published in referenced scientific journals. The diversity in the data base, unavoidably, percolates our analysis. However, to minimize variations from compilation, the data scanned from the original publications were digitized and consolidated by reiteration and by averaging out small variations. Nonconspicuous data points were ignored. Generally, the original data sources used in this work do not report error bars. Experience with quantitative stereological techniques suggests that  $\pm 10$  pct relative error is not an unreasonable estimate of errors associated with such measurements. Of course, in some cases, one can obtain errors less than this, say,  $\pm 5$  pct, but in many cases, errors can be larger, say,  $\pm 20$  pct, particularly for quantities that are derived from the ratio of two measured quantities. We believe  $\pm 10$  pct error in the absence of data is a reasonable guide, and we inserted error bars corresponding to this to all data obtained by stereological techniques or any result from expressions that take a stereological quantity, e.g.,  $V_V$ , as input. It is worthy of note that both our calculated  $R^2$  values and the visual inspection of our graphs that follow suggest that the error might be less than this estimate. A smaller error would highlight the good fit of the models presented subsequently.

Nonetheless, owing to the lack of available information from the data sources, we decided to use what are probably conservative error bars.

#### IV. DRIVING FORCE INDUCED TRANSFORMATION

The driving force increases as the temperature decreases. The martensite volume fraction obtained by continuous cooling below the martensite start temperature,  $M_s$ , results from athermal or anisothermal transformation.<sup>[35]</sup> However, Xie *et al.*<sup>[36]</sup> were able to induce plate martensite formation at constant temperature in Fe-21.5 mass pct Ni-0.95 mass pct C, a typical ‘‘athermal alloy,’’ starting with *single crystals* cooled under hydrostatic pressure to stabilize the austenite down to a fixed temperature. Then, by releasing the pressure to increase driving force, martensite was obtained at constant temperature. The martensite volume fraction as a function of pressure is reported in Reference 36. To take into consideration the effect of hydrostatic pressure on the density of nucleation sites at constant temperature, ignoring the effect of pressure on volume change,<sup>[11]</sup> Eq. [9] is recast:

$$n_V^{T,\Pi} = 2a_{ac}S_{V,m}(1 - V_V)\varepsilon_B v_m \left(\frac{\Pi - \Pi_{0,T}}{RT}\right) \quad [13]$$

where  $\varepsilon_B$  is the Bain strain,  $v_m$  is the molar volume,  $\Pi$  stands for pressure, and  $\Pi_{0,T}$  is the critical pressure for transformation to start at temperature  $T$ . Furthermore, replacing  $\xi$  by  $\Pi$  (pressure) in Eq. [10],  $\frac{d\xi}{\xi} = \frac{d\Pi}{\Pi}$ , recalling that  $A = \frac{96a_{ac}}{\pi S_{V,\gamma}^2}$ , and integrating obtains

$$I_{\Pi}(V_V) = \int_{V_{V,1}}^{V_V} \frac{9\pi \exp\left(\frac{9\pi V_V}{16\alpha}\right)}{16\alpha(\exp\left(\frac{3\pi V_V}{16\alpha}\right) - 1)} dV_V = \Xi \left(\Pi \cdot \Pi_{0,T} - \frac{\Pi^2 + \Pi_{0,T}^2}{2}\right) = \Xi P(\Pi) \quad [14]$$

where  $V_{V,1}$  is the fraction transformed at  $\Pi_{0,T}$ . The term  $\Xi$  is defined by

$$\Xi = \frac{\Xi_0}{T} \exp\left(-\frac{E_p}{kT}\right) \quad [15]$$

and  $\Xi_0$  by

$$\Xi_0 = \frac{96a_{ac}}{\pi S_{V,\gamma}^2} \left(\frac{v\varepsilon_B v_m}{R\Pi}\right) \quad [16]$$

where  $\Xi$  is given in units of pressure<sup>2</sup> and  $\Xi_0$  in units of temperature  $\times$  pressure<sup>-2</sup>.

The experimental data from Reference 36 were fitted with Eq. [14], using  $\Xi$  as a fitting parameter, as shown in Figure 2. The slopes of the lines through the data points ( $\Xi$  values) are negative, because increasing driving force is achieved by decreasing the pressure. Values of  $\Xi$  in the range 0.38 to 0.58 indicate cooperative plate arrangements typical in bursting alloys.<sup>[37]</sup> The determination coefficient ( $R^2$ ) is significantly higher than 0.90, as can be observed in Table I, where a summary of the numerical

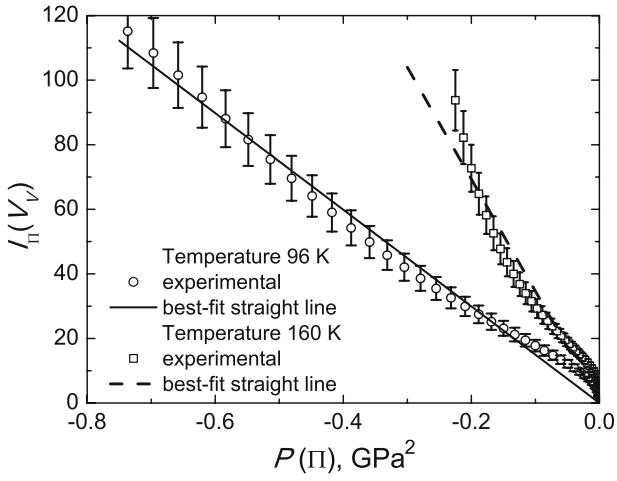


Fig. 2—Martensite induced by a decrease in hydrostatic pressure. Data from Xie *et al.*<sup>[36]</sup> plotted after Eq. [14].  $I_{II}(V_V) = \int_{V_V}^{V_V} \frac{9\pi \exp(\frac{9\pi V_V}{16\alpha})}{16\alpha (\exp(\frac{3\pi V_V}{16\alpha}) - 1)} dV_V$  and  $P(\Pi) = \Pi \cdot \Pi_{0,T} - \frac{\Pi^2 + \Pi_{0,T}^2}{2}$  (for details, see Eq. [14]).

**Table I. Analysis of Data from Driving Force-Induced Martensite**

$\dot{\Pi}$ , GPa·s <sup>-1</sup>	4.17·10 <sup>-4</sup>		2.50·10 <sup>-3</sup>
Temperature, K	160	96	147
$\Xi$ , GPa <sup>-2</sup>	346.8	149.7	296.9
$\alpha$	0.38	0.49	0.58
$R^2$	0.94	0.99	0.97
$E_p$ , J·event <sup>-1</sup>	4.33·10 <sup>-21</sup>		—
$\Xi_0$ , K·GPa <sup>-2</sup>	4.24·10 <sup>5</sup>		—

parameters can be found. Unfortunately, not every data set shown in Reference 36 was acquired under the same rate of pressure release. Hence, only the  $\Xi$  values from transformation at 96 and 160 K with the rate of pressure release of 4.17·10<sup>-4</sup> GPa·s<sup>-1</sup>, Figure 2, were used to calculate  $E_p$  and  $\Xi_0$ . The apparent activation energy so obtained,  $E_p = 4.33 \cdot 10^{-21}$  J·event<sup>-1</sup>, compares with that obtained from isothermal martensite in FeNiMn at atmospheric pressure,<sup>[19,20]</sup> as well as with the 8.24·10<sup>-21</sup> J·event<sup>-1</sup> reported by Pietikäinen<sup>[38]</sup> with a different model. This convergence of  $E_p$  values will be observed in other instances as well. From the value of  $\Xi_0 = 4.24 \cdot 10^5$  K·GPa<sup>-2</sup>, we obtained  $a_{ac} = 1.8 \cdot 10^{-8}$  m<sup>-2</sup>. For that, we used  $R = 8.3$  J·K<sup>-1</sup> mol<sup>-1</sup>,  $\epsilon_B = 0.03$ , and  $v_m = 7.1 \cdot 10^{-6}$  m<sup>3</sup> from Reference 38, and  $S_V = 883$  m<sup>-1</sup> estimated from the dimensions of the crystals used in the experiment. It is worthy of note that the value of  $a_{ac}$  is much smaller than 1.4·10<sup>-2</sup> m<sup>-2</sup> obtained with FeNiMn isothermally transformed at ambient pressure.<sup>[20]</sup> The reason for this is not straightforward. The magnitude of the hydrostatic pressure used in the experiments (1.5 GPa) is well above the atmospheric pressure: 10<sup>-4</sup> GPa. Our estimate of  $S_V$  did not take internal boundaries into consideration. Notwithstanding, it is apparent that thermal activation could also be effective in martensite formed at temperatures approaching the martensite start temperature. The

existence of common fundamentals between time-dependent and time-independent modes of martensite transformation has been already pointed out in Reference 39.

## V. TRANSFORMATION UNDER MAGNETIC FIELD

The chemical driving force for martensite transformation in iron alloys is affected by magnetic field<sup>[40]</sup> and so is the transformation curve. The experiments described by San Martin *et al.*<sup>[41]</sup> demonstrate the influence of an external magnetic field on the time-dependent martensite transformation in a Fe-12 mass pct Cr-9 mass pct Ni-4 mass pct Mo-2 mass pct Cu steel. However, the small austenite grain size  $\approx 6$  to 8·10<sup>-3</sup> mm reported in Reference 41 permits assuming transformation under spread. Since a magnetic field affects both  $\Delta G$  and  $\Delta G_0$ , the effect on their difference is null. Equation [12] can be directly used to analyze their data, after replacing  $\xi$  by time,  $t$ , and noticing that  $\frac{d\xi}{\xi} = \frac{dt}{t}$ . Integration between times  $t_1$  and  $t$  to avoid the  $\xi$  complication of incubation time gives us

$$I_{mag}(V_V) = \ln\left(\frac{1 - V_{V,1}}{1 - V_V}\right) = \sigma_S(T)v(t - t_1) \quad [17]$$

where  $\sigma_S$  is defined by

$$\sigma_S(T) = A^S \frac{\Delta S T^* - T}{k} \exp\left(-\frac{E_p}{kT}\right) \quad [18]$$

where  $A^S = n_V^0 a_{ac}^s \bar{v}$ .

The data from Fe-12 mass pct Cr-9 mass pct Ni-4 mass pct Mo-2 mass pct Cu heat treated and transformed under field strengths of 2 and 4 T<sup>[41]</sup> were fitted ( $v = 10^{13}$  s<sup>-1</sup>) to Eq. [17], (Figure 3). The values of  $\sigma_S(T)$  from Table II were used in an Arrhenius plot (not shown) to obtain the apparent activation energy,  $E_p$ . The term  $T^*$  was used as a fitting parameter, and  $\frac{\Delta S}{k} \approx 0.5$ .<sup>[42]</sup> Similar values of  $T^*$ , 254 K at 2 T and 256 K at 4 T, yielded a determination coefficient ( $R^2$ )

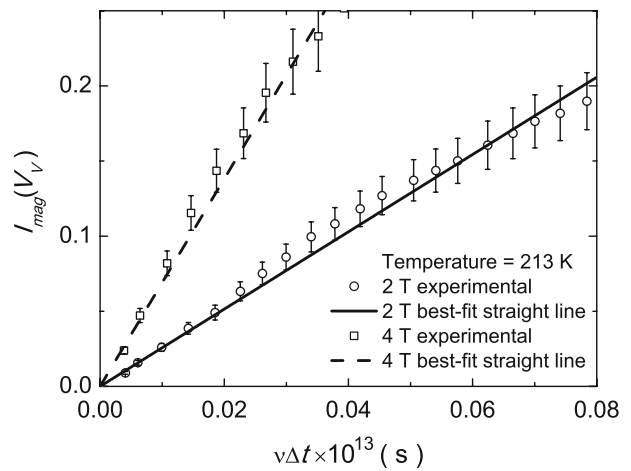


Fig. 3—Martensite transformation at 213 K under 2 and 4 T magnetic field. Data from San Martin *et al.*<sup>[41]</sup> plotted after Eq. [17],  $I_{mag}(V_V) = \ln\left(\frac{1 - V_{V,1}}{1 - V_V}\right)$  and  $\Delta t = t - t_1$ .

**Table II. Analysis of Data from Heat-Treated Fe-12 Mass Pct Cr-9 Mass Pct Ni-4 Mass Pct Mo-2 Mass Pct Cu Steel**

Field Strength, $T$	2			4		
Temperature, K	213	233	253	213	233	253
$\sigma_s(T) \times 10^{13}$	2.57	3.07	1.03	6.90	10.0	2.33
$R^2$	0.98	0.97	0.96	0.94	0.81	0.99
$E_p, \text{J}\cdot\text{event}^{-1}$	$3.5 \cdot 10^{-20}$			$4.5 \cdot 10^{-20}$		
$A^S$	$4.3 \cdot 10^{-7}$			$3.8 \cdot 10^{-5}$		

better than 0.90. The values of  $E_p$  and  $A^S$  are shown in the bottom of Table II.

Unfortunately, the values of  $a_{ac}^s$  and  $\bar{v}$  are not known, hindering calculation of  $n_V^0$  from  $A^S$ .

## VI. STRAIN-INDUCED MARTENSITE

In this section, we are concerned with martensite formed during plastic deformation of some steels, *e.g.*, stainless steels<sup>[44,45]</sup> and high-strength low-alloy steels (HSLA).<sup>[46]</sup>

The details of the microstructure of strain-induced martensite in stainless steel and HSLA are difficult to quantify. The martensite units are very small and the assumption of a constant mean martensite plate volume,  $\bar{v}$ , is acceptable,<sup>[42]</sup> so that  $V_V = \bar{v}N_V$  can be used instead of Eq. [7]. It is also generally accepted that deformation debris include potential nucleation sites, such as shear band intersections.<sup>[42,47,48]</sup> *Ad hoc*,  $n_V^T$  will be expressed by the product  $N(\varepsilon)\frac{\Delta G - \Delta G_0}{kT}$ , where  $N(\varepsilon)$  gives the strain ( $\varepsilon$ ) dependence of the density of the potential nucleation sites (including the autocatalytic ones). Henceforth, it can be shown that the following equation should describe the strain-induced martensite transformation curve, if thermal activation is effective:

$$\ln\left(\frac{1 - V_{V,1}}{1 - V_V}\right) = \frac{v}{\xi} \frac{\Delta G - \Delta G_0}{kT} \exp\left(-\frac{E_p}{kT}\right) \bar{v} \int_{\varepsilon_1}^{\varepsilon} N(\varepsilon) d\varepsilon \quad [19]$$

where  $\xi$  is the strain rate and the other terms are as defined previously. The integral in Eq. [19] may be evaluated from  $(V_{V,1}, \varepsilon_1)$  to  $(V_V, \varepsilon)$  to avoid the complication of the initial condition. The term  $\varepsilon_1$  is the strain at which a meaningful volume fraction of martensite,  $V_{V,1}$ , is obvious. Analyzing  $\ln\left(\frac{1 - V_{V,1}}{1 - V_V}\right)$  as a function of  $\varepsilon$  at constant temperature allows fetching  $N(\varepsilon)$ .  $N(\varepsilon) = n_e \varepsilon^m$  fits purpose. The term  $n_e$  is given in sites per unit volume, and  $m$  is unitless.

Substitution into Eq. [19] yields

$$I_\varepsilon(V_V) = \ln\left(\frac{1 - V_{V,1}}{1 - V_V}\right) = \sigma_\varepsilon(T) \int_{\varepsilon_1}^{\varepsilon} \varepsilon^m d\varepsilon \quad [20]$$

where

$$\sigma_\varepsilon(T) = \frac{v}{\xi} \frac{\Delta G - \Delta G_0}{kT} \exp\left(-\frac{E_p}{kT}\right) \bar{v} n_e \quad [21]$$

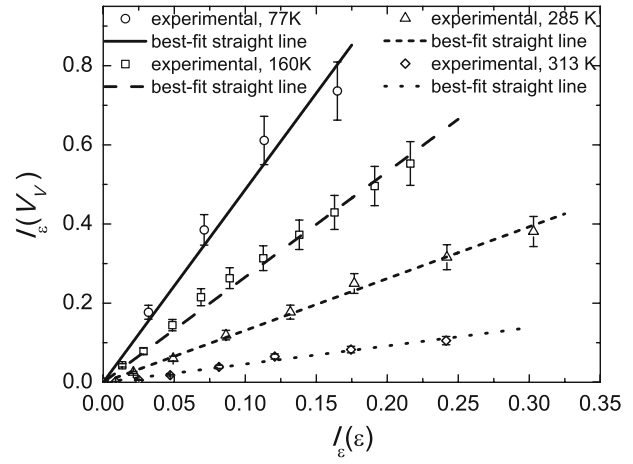


Fig. 4—Strain-induced transformation in AISI 304,<sup>[45]</sup> as described by the model in Eq. [20]. The determination coefficient ( $R^2$ ) is 0.96 or better. Values of  $m$  are given in Table III.  $I_\varepsilon(V_V) = \ln\left(\frac{1 - V_{V,1}}{1 - V_V}\right)$  and  $I_\varepsilon(\varepsilon) = \int_{\varepsilon_1}^{\varepsilon} \varepsilon^m d\varepsilon$  (for details, see Eq. [20]).

**Table III. Average Composition of Ni-Cr Steels<sup>[44]</sup> in Mass Percent: (a) Steel I from Angel<sup>[44]</sup> and (2) Steel II from Shin *et al.*<sup>[45]</sup>**

Steel	C	Si	Mn	Cr	Ni	Mo	Ni <sub>eq</sub> , Mass Pct
I	0.135	0.44	0.44	17.30	7.4	0.30	22.35
II	0.085	0.56	1.05	18.07	8.5	0.18	21.22

**Table IV. Results from Fitting Equation [20] to Ni-Cr Steels**

$T, \text{K}$	Steel I <sup>[44]</sup>			Steel II <sup>[45]</sup>			
	$\sigma_\varepsilon(T)$	$m$	$R^2$	$T, \text{K}$	$\sigma_\varepsilon(T)$	$m$	$R^2$
85	27.67	0.5	0.97	77	4.87	0.5	0.97
203	9.33	0.5	0.98	206	4.12	0.5	0.99
243	12.79	0.5	0.99	223	3.56	0.5	0.96
273	5.56	0.5	0.94	243	2.66	0.5	0.99
283	3.75	0.5	0.94	278	1.34	0.5	0.99
295	5.08	2	0.97	285	1.31	1	0.99
—	—	—	—	301	0.53	1	0.99
—	—	—	—	313	0.46	2	0.98

Inspection of Figure 4 and Table IV indicates that transformation data from the steels listed in Table III can be described by Eq. [20], using  $m$  as the fitting parameter. It is worth noting that  $m \geq 0$  and increases abruptly at high temperatures, as  $T \rightarrow T^*$ . This could be expected since generation of strain induced embryos would be less favorable as  $\Delta G \rightarrow \Delta G_0$ , demanding more mechanical stimulus.<sup>[45]</sup> Inspection of Table IV also discloses that  $\sigma_\varepsilon(T)$  appears more affected than  $m$  upon switching from steel I to steel II. These values of  $\sigma_\varepsilon(T)$  from Table IV were used in an Arrhenius plot to fetch thermal activation, by rearranging Eq. [21]:

$$\ln\left(\frac{kT}{\Delta S T^* - T} \sigma_\varepsilon(T)\right) = \ln\left(\frac{v}{\xi} n_e \bar{v}\right) - \frac{E_p}{kT} \quad [22]$$

**Table V. Other Model Parameters from Fitting Equation [19] to Ni-Cr Steels**

Steel	$\dot{\epsilon}$ , s <sup>-1</sup>	$n_e \bar{v}$	$E_p$ , J-event <sup>-1</sup>	$R^2$	$T^*$ , K	Ni <sub>eq</sub> , Mass Pct
I	1.0·10 <sup>-3</sup>	1.5·10 <sup>-15</sup>	2.5·10 <sup>-21</sup>	0.94	315	22.35
II	4.2·10 <sup>-3</sup>	5·10 <sup>-14</sup>	2.2·10 <sup>-21</sup>	0.68	321	21.22

**Table VI. Strain Induced Transformation in HSLA Steel\*;<sup>[51]</sup> Parameters from Equation [20]**

$\dot{\epsilon}$ , s <sup>-1</sup>	$T$ , K	$\sigma_\epsilon(T)$	$m$	$R^2$
3.33·10 <sup>-2</sup>	298	0.53	0	0.81
3.33·10 <sup>-2</sup>	423	0.11	0	0.92
3.33·10 <sup>-5</sup>	298	0.57	0	0.84
3.33·10 <sup>-5</sup>	423	0.58	0	0.99

\*Composition in mass pct: Fe-0.040C-0.49Si-1.48Mn- 0.96Al-0.10-Mo-0.024Nb-0.0009S-0.0005N.

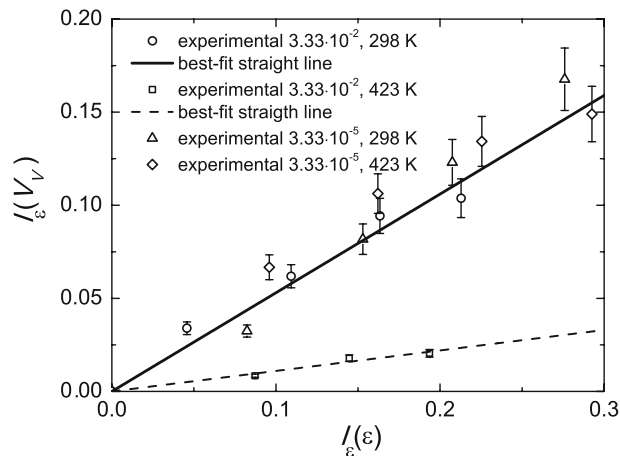


Fig. 5—HSLA steel data<sup>[51]</sup> plotted after the model Eq. [20] with high fitting determination coefficient.  $I_\epsilon(V_V) = \ln\left(\frac{1-V_V}{1-V_V^0}\right)$  and  $I_\epsilon(\epsilon) = \int_{\epsilon_0}^{\epsilon} e^m d\epsilon$  (for details see Eq. [20]).

The plot of the data after Eq. [22] can be linearized by fitting  $T^*$  and using  $\Delta S/k \approx 0.5$ .<sup>[42]</sup> The resulting  $E_p$  values support the conclusion that thermal activation is also effective in strain induced martensite. Moreover, the magnitude of the apparent activation energy values listed in Table V compares with that obtained from the initial rate of martensite transformation in FeNiMn<sup>[19]</sup> as well as with the value obtained in Section IV. Also, the values of  $T^*$  correlate with the austenite stability estimated by the value of Ni<sub>eq</sub>,<sup>[49]</sup> as might be expected (Table V). Unfortunately, the values of  $\bar{v}$  are not known, so the parameter  $n_e$  cannot be discussed at this time.

Strain-induced martensite transformation in a HSLA steel with martensite-austenite microstructure is described by Mukherjee *et al.*<sup>[50,51]</sup> Using the data reported by Mukherjee *et al.*, martensite volume fraction was calculated considering an initial untransformed austenite fraction of 0.2. The graphs in Figure 5 show that Eq. [20], with  $m = 0$  describes the data with high determination coefficient. The slope of the fitted lines,  $\sigma_\epsilon(T)$  values in Table VI, shows that the temperature and strain rate have opposite effects on  $\sigma_\epsilon(T)$ , as expected in a thermally activated process. However, with just one pair of values of  $\sigma_\epsilon(T)$  and two strain rates, 3.33·10<sup>-2</sup> s<sup>-1</sup> and 3.33·10<sup>-5</sup> s<sup>-1</sup>, it is not possible to use correlation analysis to check thermal activation using an Arrhenius plot. Notwithstanding that, by adjusting  $T^*$  in Eq. [22], it was possible to obtain a similar activation energy,  $E_p = 5 \cdot 10^{-20}$  J-event<sup>-1</sup>, from either data pair. The values of  $T^*$  were 424 K at the higher strain rate

and 428 K at the lower strain rate. It is seen that  $T^*$  is not much affected by strain rate; however, the product  $n_e \bar{v}$  varies from 1.4·10<sup>-12</sup> to 1.2·10<sup>-9</sup>, a factor of 10<sup>3</sup>, the same ratio of the imposed strain rate, 3.33·10<sup>-5</sup> and 3.33·10<sup>-2</sup>. A possible significant effect of the strain rate on  $n_e$  cannot be dismissed at this time. In fact, this is a topic that deserves further investigation, because many steels designed to benefit from strain-induced martensite (TRIP steels) endure high strain-rate deformation in processing or usage.

## VII. DISCUSSION

In previous work, a unified model was presented for the initiation<sup>[19]</sup> and subsequent martensite transformation.<sup>[20]</sup> These are described in Sections II and III, respectively.

The main model results used in this work are Eqs. [10] and [12], which describe martensite transformation when “fill in” or “spread” predominates, respectively. Equations [10] and [12] are written as a function of a progress variable  $\zeta$ . In Guimarães and Rios,<sup>[20]</sup>  $\zeta$  was identified with temperature  $T$  for athermal martensite transformation in a FeNiC alloy and with  $t$  for isothermal transformation in a FeMnNi alloy. In both cases, martensite transformation could be successfully described by the unified model (References 19 and 20 provide details).

In this work, we took the unified model a step further, showing that the same formalism can also be successfully applied when isothermal martensite transformation takes place under a magnetic field,  $\zeta = t$ , or is driven by a decrease in hydrostatic pressure,  $\zeta = \Pi$ , or is induced by applied strain,  $\zeta = \epsilon$ . In each case, a good agreement was obtained between the model equations and experimental data with a reasonably high coefficient of determination,  $R^2$ . This can be seen from the results depicted in Figures 2 through 5. A summary of numerical results for all data can be found and is summarized in Tables I through VI.

The unified model is a formal or phenomenological model. Therefore, even though its parameters are related to the physics of the transformation, no specific mechanisms were assumed. As a consequence, the values of the parameters obtained by fitting such diverse martensitic transformations may reflect different underlying mechanisms. Thus, large differences in one parameter from one reaction to another might indicate a significant change in underlying mechanism. By contrast, the lack



of such a difference, or the fact that the difference is relatively small, might well mean that the underlying mechanism might be the same for the alloys analyzed.

Two key features of martensite transformations, autocatalysis and activation energy, were taken into consideration by the model and a specific parameter was assigned to each of them. Namely,  $a_{ac}$  or  $\alpha'_{ac}$  for autocatalysis and  $E_p$  for activation energy.

By factoring the kinetic equation into an athermal (driving force dependent) factor,  $\frac{\Delta G - \Delta G_0}{kT}$ , and a thermal activation factor expressed by the Boltzmann factor, we obtained values of apparent activation energy,  $E_p$ , within an order of magnitude. These  $E_p$  values are compatible with previous results of the activation energy for martensite nucleation found in the literature. This finding strongly suggests that a similar barrier regulates martensite transformation induced by different means in the various alloys at constant temperature. Moreover, the small values of  $E_p$  imply a barrier smaller than the classical barrier for a single-domain nucleus. It is a contention that the similar  $E_p$  values express qualitative agreement with the view that martensite nucleation comprises an austenite defect that catalyzes embryo formation.<sup>[54–56]</sup> The embryo→nuclei transition occurs barrierless or could be regulated by a small barrier overcome by thermal activation.<sup>[14]</sup> Moreover, the small values of  $E_p$  imply a smaller barrier than that calculated for the classical barrier of a single-domain nucleus. The ratio  $\frac{\Delta G - \Delta G_0}{kT}$  inferred from the small particle data<sup>[21]</sup> is consistent with a time-independent generation of embryos.

Comparing the values of the autocatalytic parameter obtained for the diverse martensitic transformations studied here, it can be seen that they differ by several orders of magnitude. However, lack of experimental data (number per unit volume of martensite units and area of martensite-austenite interfaces) hindered further analysis of the microstructural and geometrical aspects of this topic. For instance, in certain cases, one has spread in another fill in predominates. Also, the plate size may vary or not depending of the transformation, and therefore not be directly comparable. It is not unreasonable that such large differences might be compounded by different patterns of transformation strain accommodation in the austenite. Miyamoto *et al.*<sup>[52]</sup> have shown that the accommodation of the shape strain of an isolated martensite plate in the austenite depends on the morphology of the martensite unit, namely, plate, lath, or thin plate. It is plausible that accommodation is also influenced by the plate arrangement, which in turn is affected by the austenite grain size and fraction transformed. Moreover, since the generation of autocatalytic sites is expected to relate to the propagation of the martensite-austenite interface, the dynamics of the motion of the austenite-martensite interface is relevant, as discussed by Grujici and Olson.<sup>[53]</sup> Drag effects from phonon and electron as well as from the interaction of the interface with obstacles in the austenite may not be identical in all alloys. Also, we assumed  $\nu = 10^{13} \text{ s}^{-1}$ , although the effective frequency of nucleation attempts may be less.<sup>[9,35,57]</sup>

## VIII. CONCLUSIONS

1. By factoring the martensite reaction rate into an athermal factor (driving force dependent, inferred from small FeNi particles transformed by quenching) and a thermally activated factor expressed by the Boltzmann factor, a formal kinetic model was developed to describe martensite transformation in Fe-base alloys.
2. The formal theory proposed by the present authors<sup>[19,20]</sup> to describe the martensite transformation curves allows a unified description of martensite transformation kinetics in iron alloys. Martensite transformations, including athermal, isothermal, isothermal induced by depressurization, magnetic field, and applied strain, could all be described within the framework of the proposed formalism.
3. The values of the activation energy,  $E_p$ , obtained for every constant temperature reaction analyzed here fall roughly within an order of magnitude and are compatible with the results found in the literature. We could not find that  $E_p$  follows any obvious composition dependence. These results support the contention that  $E_p$  refers not to a classical nucleation barrier, but to some step along the reaction path.
4. Moreover, the phenomenological analysis suggested that the driving force due to chemical and non-chemical factors may affect the intensity of nucleation events.
5. These findings are qualitatively compatible with the view that in a favorable environment, austenite evolves into embryos that, eventually, are promoted to nuclei, that propagate into a full martensite unit. The embryo→nuclei transition may be barrierless or regulated by a small barrier overcome by thermal activation.

## ACKNOWLEDGMENTS

One of the authors (PRR) is grateful to Conselho Nacional de Desenvolvimento Científico e Tecnológico, CNPq, and to Fundação de Amparo à Pesquisa do Estado do Rio de Janeiro, FAPERJ, for the financial support. Thanks are due to Professor H. Goldenstein (USP-SP) for his valuable assistance with the bibliography.

## REFERENCES

1. J.C. Fisher, J.H. Hollomon, and D. Turnbull: *Trans. AIME*, 1949, vol. 185, pp. 691–700.
2. M. Cohen, E.S. Machlin, and V.G. Paranjpe: *Thermodynamics in Physical Metallurgy*, ASM, Cleveland, OH, 1949, pp. 242–65.
3. H. Knapp and U. Dehlinger: *Acta Metall.*, 1956, vol. 4, pp. 289–97.
4. L. Kaufman and M. Cohen: *Progr. Met. Phys.*, 1958, vol. 7, pp. 165–246.
5. G.B. Olson: Sc.D. Thesis, MIT, Cambridge, MA, 1974.
6. M.A. Meyers: *Acta Metall.*, 1980, vol. 28, pp. 757–70.
7. A. Shibata, S. Morito, T. Furuhashi, and T. Maki: *Acta Mater.*, 2009, vol. 57, pp. 483–92.
8. G. Ghosh and G.B. Olson: *Acta Mater.*, 1994, vol. 42, pp. 3361–70.
9. C.L. Magee: in *Phase Transformations*, H.I. Aaronson, ed., ASM, Cleveland, OH, 1968, pp. 115–56.



10. K. Kakeshita, K. Kuroiwa, T. Ikeda, A. Yamagishi, A. Date, and K. Shimizu: *Mater. Trans. JIM*, 1993, vol. 34, pp. 423–28.
11. T. Kakeshita and K. Shimizu: *Mater. Trans. JIM*, 1997, vol. 38, pp. 668–81.
12. T. Kakeshita, T. Fukuda, and T. Saburi: *Sci. Technol. Adv. Mater.*, 2000, vol. 1, pp. 63–72.
13. A.L. Roitburd: *Mater. Sci. Eng. A*, 1990, vol. 127, pp. 229–38.
14. W. Zang, Y.M. Jin, and A.G. Khachaturyan: *Acta Mater.*, 2007, vol. 55, pp. 565–74.
15. C. Shen, J. Li, and Y. Wang: *Mater. Metall. Trans. A*, 2008, vol. 39A, pp. 976–83.
16. D.E. Laughlin, N.J. Jones, A.J. Schwartz, and T.B. Massalski: Carnegie-Mellon University, Pittsburgh, PA, personal communication, 2008.
17. P.R. Rios and J.C. Guimarães: *Scripta Mater.*, 2007, vol. 57, pp. 1105–08.
18. P.R. Rios and J.C. Guimarães: *Mater. Res.*, 2008, vol. 11, pp. 103–08.
19. J.C. Guimarães and P.R. Rios: *J. Mater. Sci.*, 2008, vol. 43, pp. 5206–10.
20. J.R.C. Guimarães and P.R. Rios: *J. Mater. Sci.*, 2008, vol. 44, pp. 998–1005.
21. R.E. Cech and D. Turnbull: *Trans. AIME*, 1956, vol. 206, pp. 124–32.
22. M. Cohen and G.B. Olson: *Suppl. Trans. JIM*, 1976, vol. 17, pp. 93–98.
23. A. Borgenstam and M. Hillert: *Acta Mater.*, 1997, vol. 45, pp. 651–62.
24. G. Ghosh and V. Raghavan: *Mater. Sci. Eng. A*, 1986, vol. 80A, pp. 65–74.
25. G.V. Kurdjumov and O.P. Maximova: *Dokl. Akad. Nauk. SSSR*, 1948, vol. 61, pp. 83–87.
26. G.V. Kurdjumov and O.P. Maximova: *Dokl. Akad. Nauk. SSSR*, 1950, vol. 73, pp. 95–98.
27. V. Raghavan: *Acta Metall.*, 1969, vol. 17, pp. 1299–1303.
28. D.G. McMurtrie and C.L. Magee: *Metall. Trans.*, 1970, vol. 1, pp. 3185–91.
29. J.C. Guimarães: *Mater. Sci. Technol.*, 2008, vol. 24, pp. 843–47.
30. V. Raghavan and A.R. Entwisle: *Physical Properties of Martensite and Bainite*, ISI Special Report 93, Iron and Steel Institute, London, 1965, p. 30.
31. S.R. Pati and M. Cohen: *Acta Metall.*, 1971, vol. 19, pp. 1327–32.
32. J.W. Christian: *Physical Properties of Martensite and Bainite*, ISI Special Report 93, Iron and Steel Institute, London, 1965, p. 43.
33. A.R. Entwisle: *Physical Properties of Martensite and Bainite*, ISI Special Report 93, Iron and Steel Institute, London, 1965, p. 43.
34. V.I. Levitas, A.V. Idesman, G.B. Olson, and E. Stein: *Phil. Mag.*, 2002, vol. 82, pp. 429–62.
35. M.F. Lin, G.B. Olson, and M. Cohen: *Metall. Trans. A*, 1992, vol. 23A, pp. 2987–97.
36. Z.L. Xie, B. Sundqvist, H. Hänninen, and J. Pietikäinen: *Acta Metall. Mater.*, 1993, vol. 41, pp. 2283–90.
37. J.C. Guimarães and J.C. Gomes: *Proc. Int. Conf. of Martensitic Transformations*, MIT, Cambridge, MA, 1979, pp. 59–64.
38. J. Pietikäinen: *Acta Metall. Mater.*, 1995, vol. 43, pp. 2667–71.
39. T. Kakeshita, J. Katsuyama, T. Fukuda, and T. Saburi: *Mater. Sci. Eng. A*, 2001, vol. 312, pp. 219–26.
40. T. Kakeshita, K. Shimizu, T. Sakakibara, S. Fukuda, and M. Date: *Trans. JIM*, 1983, vol. 24, pp. 748–53.
41. D. San Martin, K.W.P. Aarts, P.J. Rivera-Diaz-del-Castillo, N.H. van Dijk, and S. van de Zwaag: *J. Magn. Magn. Mater.*, 2008, vol. 320, pp. 1722–28.
42. G.B. Olson and M. Cohen: *Metall. Trans. A*, 1975, vol. 6A, pp. 791–95.
43. Y.V. Kalentina, V.M. Schastlivtsev, and E.A. Fokina: *Met. Sci. Heat Treatment*, 2008, vol. 50, pp. 164–70.
44. T. Angel: *J. Iron Steel Inst.*, 1954, vol. 177, pp. 165–74.
45. H.C. Shin, T.K. Ha, and Y.W. Chang: *Scripta Mater.*, 2001, vol. 45, pp. 823–29.
46. *International Conference on TRIP-Aided High Strength Ferrous Alloys*, B.C. De Cooman, ed., Steel GRIPS, 2002, vol. 1, pp. 1–382.
47. M.A. Meyers, B.Y. Cao, V.F. Nesterenko, D.J. Benson, and Y.B. XU: *Metall. Mater. Trans. A*, 2004, vol. 35A, pp. 2575–85.
48. J. Talonen and H. Hanninen: *Acta Mater.*, 2007, vol. 55, pp. 6108–18.
49. T. Hirayama and M. Ogirima: *J. Jpn. Inst. Met.*, 1970, vol. 34, pp. 507–10.
50. M. Mukherjee, S.B. Singh, and O.N. Mohanty: *Metall. Mater. Trans. A*, 2008, vol. 39A, pp. 2320–28.
51. M. Mukherjee, O.N. Mohanty, S. Hashimoto, T. Hojo, and K. Sugimoto: *ISIJ Int.*, 2006, vol. 46, pp. 316–24.
52. G. Myamoto, A. Shibata, T. Maki, and T. Furuhashi: *Acta Mater.*, 2009, vol. 57, pp. 1120–31.
53. M. Grujicic and G.B. Olson: *Interface Sci.*, 1998, vol. 9, pp. 155–64.
54. J.W. Christian: *The Institute of Metals Monograph Series No. 33* (London), 1969, p. 129.
55. J.R.C. Guimaraes and D.L. Valeriano Alves: *Phil. Mag.*, 1974, vol. 30, pp. 277–83.
56. G.B. Olson and M. Cohen: *Metall. Trans. A*, 1976, vol. 7, pp. 1905–14.
57. C.L. Magee: *Metall. Trans.*, 1971, vol. 2, pp. 2419–30.